Electrochemical and Solid-State Letters, **13** (10) H357-H359 (2010)
1099-0062/2010/13(10)/H357/3/$28.00 © The Electrochemical Society

Postannealing Process for Low Temperature Processed Sol–Gel Zinc Tin Oxide Thin Film Transistors

Seok-Jun Seo, Young Hwan Hwang, and Byeong-Soo Bae[z]

Laboratory of Optical Materials and Coating, Department of Materials Science and Engineering, Korea Advanced Institute of Science and Technology, Daejeon 305-701, Korea

We fabricated zinc tin oxide (ZTO) thin film transistors (TFTs) using a stable ZTO sol–gel solution at a low annealing temperature of 300°C. To enhance transistor performance, the ZTO films were postannealed under vacuum and wet air consecutively. The vacuum and wet air postannealed ZTO TFTs exhibited high saturation mobilities (5.5 $cm^2/V\ s$), low subthreshold swing (0.38 V/dec), and high on–off current ratio (8×10^8). We analyzed the ZTO films before and after postannealing by X-ray photoelectron spectroscopy to explain the origin of the enhanced performance.
© 2010 The Electrochemical Society. [DOI: 10.1149/1.3474606] All rights reserved.

Manuscript submitted May 17, 2010; revised manuscript received June 21, 2010. Published August 6, 2010.

Recently, transparent oxide semiconductors (TOSs) have attracted a great deal of attention as the channel layer for transparent thin film transistors (TFTs) due to their high mobility, good environmental stability, low cost, high transparency, and low temperature processibility.[1,2] Among TOSs, oxides based on heavy metal cations with $(n-1)d^{10}\ ns^0$ $(n \geq 5)$ electronic configurations that have a large spatial spreading of the s-orbital for a considerable overlap between neighboring orbitals are promising candidates for high mobility channel materials, even in an amorphous state. Zinc tin oxide (ZTO),[3] indium zinc oxide,[4] zinc indium tin oxide,[5] and indium gallium zinc oxide (IGZO)[6] are representative amorphous oxide semiconductors. These amorphous oxide-based TFTs showed high mobilities of up to 40 $cm^2/V\ s$.

Most amorphous oxide semiconductors are generally prepared by vacuum processes such as radio-frequency magnetron sputtering and pulsed laser deposition. These processes, however, require costly equipment and present difficulties for the economical fabrication of large area devices even at room temperature. Compared to vacuum processes, a solution process is a simple and low cost pathway and enables large area coating with high throughput. Some researchers have reported solution-processed oxide TFTs with high mobilities ($>10\ cm^2/V\ s$) and inkjet printability.[7-9] Recently, we have reported on a ZTO TFT using a precursor solution of zinc(II) acetate and tin(II) chloride that presented high mobility and a high on–off current ratio.[10] However, a high temperature (≥ 500°C) annealing process is essential to achieve high performance in solution-processed TFTs. This high annealing temperature restricts the use of typical soda lime glass or plastic substrates for low cost electronics and is not applicable to the fabrication of large size devices. Thus, in efforts to decrease the annealing temperature of the solution-processed TFTs, several approaches such as chemical bath deposition[11] and the use of nanoparticle suspensions[12] and low temperature decomposable precursors[13] have been investigated. However, most solution-processed oxide TFTs annealed below 300°C have shown low mobility, poor subthreshold swing, and low on–off current ratios. In vacuum-processed TFTs, transistor performance could be enhanced using various postplasma treatment and postannealing processes.[14,15] In particular, it has been reported that the postannealing atmosphere affects electrical properties through control of the concentration of oxygen vacancies and electron trap sites.[15] Therefore, it is anticipated that a postannealing process for the solution-processed oxide TFTs can lower the annealing temperature.

In this article, we report on sol–gel ZTO TFTs fabricated with annealing at low temperature down to 300°C. The additional postannealing process under vacuum and wet air environments improves the transistor characteristics, yielding a high mobility of 5.5 $cm^2/V\ s$ and a high on–off current ratio of 8×10^8. Also, the mechanism underlying the enhanced performance by postannealing is discussed.

A sol–gel solution for fabricating the ZTO thin films was prepared using zinc acetate [$Zn(CH_3COO)_2$, Aldrich] and tin chloride ($SnCl_2$, Aldrich) as metal precursors and 2-methoxyethanol as a solvent. The details of the synthesis process can be found in a previous article.[10] Metal precursors in a 0.3 M concentration were dissolved in 2-methoxyethanol with an atomic ratio of Zn:Sn = 1:1. For the fabrication of bottom gate/top contact structured ZTO TFTs, the resulting solution was deposited on heavily boron (p+)-doped silicon wafers covered with a thermally grown 100 nm SiO_2 layer as a gate dielectric by spin coating at 5000 rpm for 30 s. The ZTO thin films were then annealed at 300°C for 1 h in ambient air. After the main annealing step, the samples were annealed under vacuum ($<10^{-1}$ Torr) and wet air (humidity of ~80%) atmospheres at 300°C for 1 h using a rapid thermal annealing system. Aluminum source and drain electrodes of 100 nm thick were deposited on top of the ZTO layer by E-beam evaporation via a shadow mask. The channel length and width were 100 and 1000 μm, respectively.

The structural properties of the ZTO thin films were investigated by transmission electron microscopy (TEM), X-ray diffraction (XRD) using a fixed glancing incidence angle (2°), and atomic force microscopy (AFM). The transfer characteristics of the ZTO TFTs were measured with an HP 4155A semiconductor parameter analyzer at room temperature in a dark room. To investigate the change in chemical structures of the ZTO films during postannealing, X-ray photoelectron spectroscopy (XPS) was employed.

The XRD patterns before and after the postannealing process, as shown in Fig. 1a, exhibit a weak and broad peak at 2θ = 34°. The cross-sectional TEM image and the diffraction pattern of the postannealed ZTO thin film, presented in Fig. 1b, also show no ordered

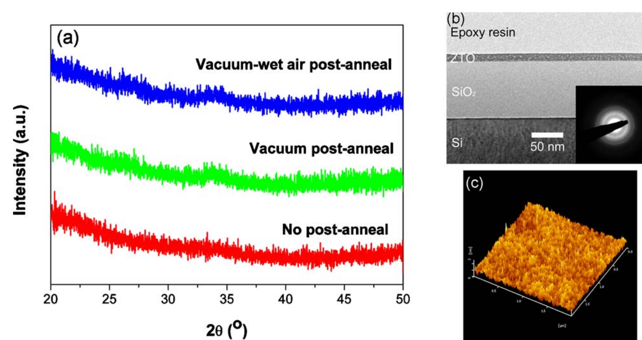

Figure 1. (Color online) (a) XRD patterns of ZTO thin films before and after postannealing, (b) cross-sectional TEM image and electron diffraction pattern (inset), and (c) AFM image of a vacuum and wet air postannealed ZTO thin film.

[z] E-mail: bsbae@kaist.ac.kr

Downloaded 13 Aug 2010 to 143.248.115.209. Redistribution subject to ECS license or copyright; see http://www.ecsdl.org/terms_use.jsp

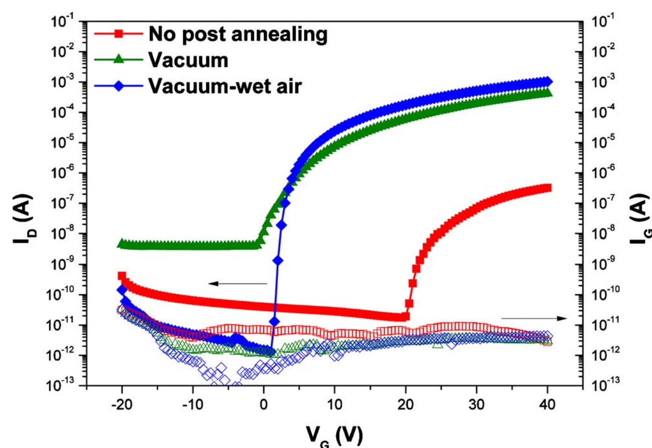

Figure 2. (Color online) Transfer characteristics (I_D: solid dot) and gate leakage current (I_G: hollow dot) at $V_{DS} = 40$ V for the ZTO TFTs before and after postannealing.

structure with uniform thickness of 15 nm. The AFM image, as shown in Fig. 1c, reveals that the postannealed ZTO film has a pinhole-free and smooth surface with a root-mean-square roughness of 0.24 nm and shows no crystal grains. These results confirm that the amorphous phase is maintained during postannealing under vacuum and wet air atmospheres.

Figure 2 shows the n-channel transfer characteristics of the drain current (I_D) vs gate voltage (V_G) and the gate leakage current behavior at a drain-to-source voltage (V_{DS}) of 40 V for the solution-processed ZTO TFTs before and after postannealing. All the TFTs show a low leakage current ($\sim 10^{-11}$ A) originating from thermally grown SiO_2 dielectric. Due to the low annealing temperature of 300°C, the TFT with the as-deposited ZTO thin film shows a low performance with a saturation mobility (μ) of 5.5×10^{-3} cm^2/V s, a subthreshold swing (S) of 1.01 V/dec, and an on–off current ratio of $\sim 1 \times 10^4$. The TFT annealed for 3 h at 300°C did not show any improvement in its characteristics (results not shown in this article) despite the longer annealing time for decomposition of the precursors. However, the TFTs with a postannealed ZTO film exhibited an enhanced performance. After vacuum postannealing, the entire I_D including the on and off current increases and the turn-on voltage (V_{on}), that is, the gate voltage at the onset of an initial sharp increase in current in the transfer curve, is negatively shifted with an increased saturation mobility of 3.17 cm^2/V s and an enhanced subthreshold swing of 1.92 V/dec. This can be explained by an increase in the carrier concentration due to the generation of oxygen vacancies, each of which donates two electrons, during the vacuum postannealing. Recently, according to first-principle calculation, it is suggested that oxygen vacancies in a multicomponent oxide such as IGZO can make deep levels as well as shallow levels, depending on its local structure.[16] Therefore, the oxygen vacancies generated during the vacuum postannealing can increase the carrier concentration. Higher carrier concentration results in conductive characteristics with increased drain current and higher saturation mobility of the ZTO TFT. However, a large number of oxygen vacancies can also act as electron trap sites in deep states,[16] and thus, the subthreshold swing is degraded after vacuum annealing. To reduce the oxygen vacancies in the vacuum-annealed TFT, we carried out wet air annealing, which provided strong oxidation conditions for amorphous oxide semiconductors.[15,17] Consecutive postannealing under a wet air atmosphere enhanced the electrical performance of the TFT, resulting in a saturation mobility of 5.5 cm^2/V s, a subthreshold swing of 0.38 V/dec, and an on–off current ratio of 8×10^8. The excess oxygen vacancies generated by vacuum annealing can be suppressed during wet air annealing, and it is expected that the decrease in the amount of oxygen vacancies, which act as sources of free carriers and defect sites, can reduce the off current and enhance the subthreshold swing. Additionally, the linear mobilities ($V_{DS} = 4$ V) of the as-deposited, vacuum postannealed, and vacuum-wet air postannealed ZTO TFTs are 2.34×10^{-3} cm^2/V s, 1.44 cm^2/V s, and 4.06 cm^2/V s, respectively. These are lower than the saturation mobilities; however, the consecutive vacuum and wet air postannealed TFT shows a comparable linear mobility, which indicates the reduction of the trap states.

For further investigation of the chemical and structural changes after postannealing, the ZTO thin films were analyzed using XPS. From the XPS spectra of the Zn $2p_{3/2}$ and Sn $3d_{5/2}$ (Fig. 3a and b), the position of the binding energy peaks and the compositional ratio of Zn and Sn atoms (Zn:Sn = 1:1) were maintained after the postannealing. However, as shown in Fig. 3c-f, the O 1s and Cl 2p peaks present remarkable changes. The O 1s peaks (Fig. 3d-f) are fitted by three nearly Gaussian curves centered at 530.1, 531.2, and 532.4 eV. The low and dominant peak of the O 1s spectrum at 530.1 eV (O_{ox}) is associated with the oxygen atoms in the fully oxidized surroundings.[18] The medium component at 531.2 eV (O_v) corresponds to oxygen ions in oxygen deficient regions. The peak with the high binding energy component at 532.4 eV (O_s) is typically attributed to the presence of loosely bound oxygen on the surface, such as in H_2O and OH groups integrated into the materials. After the vacuum annealing step, the area ratio of $O_v/(O_{ox} + O_v)$ increased from 0.19 to 0.34, which indicates that the vacuum annealing generates oxygen vacancies in the atomic structure. In addition,

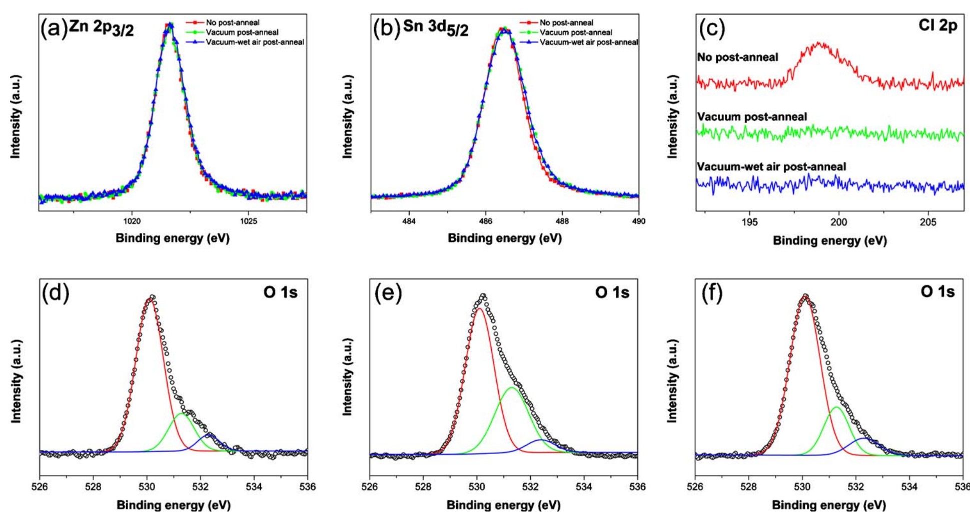

Figure 3. (Color online) XPS spectra of (a) Zn $2p_{3/2}$, (b) Sn $3d_{5/2}$, (c) Cl 2p, and O 1s of (d) as-deposited, (e) vacuum post-annealed, (f) vacuum and wet air postannealed ZTO thin films.

Downloaded 13 Aug 2010 to 143.248.115.209. Redistribution subject to ECS license or copyright; see http://www.ecsdl.org/terms_use.jsp

the Cl 2p spectra (Fig. 3c) show a significant reduction of the concentration of Cl ions from 2 to 0.4 atom %, a level that is almost undetectable after vacuum annealing. We could also confirm the reduction of the relative concentration of the Cl ions using secondary-ion mass spectrometry analysis (results not shown here). These results indicate that the drastic increase in drain current by vacuum annealing originates from high carrier concentration generated by a large amount of oxygen vacancies and a decrease in the number of defect sites from residual Cl ions. Compared with the vacuum-annealed ZTO film, the consecutive wet-air-annealed film presents a lower $O_v/(O_{ox} + O_v)$ of 0.2 with an extremely low Cl ion content. The oxygen vacancies in the ZTO film can be reduced due to the strong oxidization power of the wet air annealing process. Thus, it is confirmed that the low off current of the TFT fabricated with vacuum and wet air annealing was mainly due to a decrease in the amount of oxygen vacancies in the ZTO films.

In the solution-processed ZTO TFTs fabricated at low temperature (300°C), the overlap of the s-orbitals of heavy metal ions is insufficient despite their large radii due to a large number of impurities incorporated in the loosely structured ZTO films. The conduction band minimum (CBM), which acts as an electron pathway, is formed by the overlap of the s-orbitals.[19] Thus, the electron conduction of the ZTO film with vacuum postannealing is inevitably limited due to structural disorder, in spite of a high concentration of oxygen vacancies. However, during the wet air postannealing, metal–oxide formation and structural relaxation, which reduce the density of the shallow localized state beneath the CBM, occur due to a substantial oxidation power of the wet air atmosphere.[15,17] Therefore, the mobility can increase despite a decrease in shallow donor[20] and the subthreshold swing can be enhanced due to the decrease in trap sites.[16,21] From these postannealing effects, we suggest a plausible mechanism of the structural change during the postannealing processes. Due to the low annealing temperature, the as-deposited ZTO thin film has a large number of Cl ions and OH groups. During the vacuum postannealing, these impurities can be decomposed by the vaporization of HCl or H_2O and can eventually generate excess oxygen vacancies, which lead to a high drain current. After wet air postannealing, the oxygen vacancies are reduced and the closer metal–oxide bond formation by densification results in the enhancement of the connectivity of the s-orbital.[20,22] These changes can cause a high mobility and a low off current simultaneously in the sol–gel ZTO TFTs.

In summary, we fabricated the solution-processed ZTO TFTs at an annealing temperature of 300°C with additional postannealing under vacuum and wet air atmospheres. The vacuum postannealing step enhances the mobility by the removal of impurity ions and the generation of oxygen vacancies. The following wet air postannealing step further enhances the mobility ($5.5\ cm^2/V\ s$) with a high on–off current ratio (8×10^8) due to the metal–oxide formation and structural relaxation, despite of a decrease in the amount of the oxygen vacancies. Therefore, the postannealing process is very helpful in that it allows a reduction of the annealing temperature for the solution-processed oxide TFTs to be applicable in display manufacturing.

Acknowledgment

This research was financially supported by the Ministry of Knowledge Economy (MKE) and the Korea Institute for Advancement of Technology (KIAT) through the Human Resource Training Project for Strategic Technology. This research was also supported by the Basic Science Research Program through the National Research Foundation of Korea (NRF) funded by the Ministry of Education, Science and Technology (CAFDC-20100009898).

Korea Advanced Institute of Science and Technology assisted in meeting the publication costs of this article.

References

1. K. Nomura, H. Ohta, A. Takagi, T. Kamiya, M. Hirano, and H. Hosono, *Nature (London)*, **432**, 488 (2004).
2. R. L. Hoffman, B. J. Norris, and J. F. Wager, *Appl. Phys. Lett.*, **82**, 733 (2003).
3. H. Q. Chiang, J. F. Wager, R. L. Hoffman, J. Jeong, and D. A. Keszler, *Appl. Phys. Lett.*, **86**, 013503 (2005).
4. P. Barquinha, A. Pimentel, A. Marques, L. Pereira, R. Martins, and E. Fortunato, *J. Non-Cryst. Solids*, **352**, 1749 (2006).
5. M. K. Ryu, S. Yang, S.-H. Ko Park, C.-S. Hwang, and J. K. Jeong, *Appl. Phys. Lett.*, **95**, 072104 (2009).
6. J. K. Jeong, J. H. Jeong, H. W. Yang, J.-S. Park, Y.-G. Mo, and H. D. Kim, *Appl. Phys. Lett.*, **91**, 113505 (2007).
7. D.-H. Lee, Y.-J. Chang, G. S. Herman, and C.-H. Chang, *Adv. Mater.*, **19**, 843 (2007).
8. Y. H. Hwang, J. H. Jeon, S.-J. Seo, and B.-S. Bae, *Electrochem. Solid-State Lett.*, **12**, H336 (2009).
9. D. Kim, Y. Jeong, K. Song, S.-K. Park, G. Cao, and J. Moon, *Langmuir*, **25**, 11149 (2009).
10. S.-J. Seo, C. G. Choi, Y. H. Hwang, and B.-S. Bae, *J. Phys. D*, **42**, 035106 (2009).
11. H.-C. Cheng, C.-F. Chen, and C.-C. Lee, *Thin Solid Films*, **498**, 142 (2006).
12. S. K. Volkman, B. A. Mattis, S. E. Molesa, J. B. Lee, A. de la Fuente Vornbrock, T. Bakhishev, and V. Subramanian, *Tech. Dig. - Int. Electron Devices Meet.*, **2004**, 769.
13. S. T. Meyers, J. T. Anderson, C. M. Hung, J. Thompson, J. F. Wager, and D. A. Keszler, *J. Am. Chem. Soc.*, **130**, 17603 (2008).
14. J.-S. Park, J. K. Jeong, Y.-G. Mo, and H. D. Kim, *Appl. Phys. Lett.*, **90**, 262106 (2007).
15. K. Nomura, T. Kamiya, H. Ohta, M. Hirano, and H. Hosono, *Appl. Phys. Lett.*, **93**, 192107 (2008).
16. T. Kamiya, K. Nomura, M. Hirano, and H. Hosono, *Phys. Status Solidi C*, **5**, 3098 (2008).
17. K. Nomura, T. Kamiya, M. Hirano, and H. Hosono, *Appl. Phys. Lett.*, **95**, 013502 (2009).
18. M. Chen, Z. L. Pei, C. Sun, L. S. Wen, and X. Wang, *J. Cryst. Growth*, **220**, 254 (2000).
19. K. Nomura, T. Kamiya, H. Ohta, T. Uruga, M. Hirano, and H. Hosono, *Phys. Rev. B*, **75**, 035212 (2007).
20. S. Jeong, Y.-G. Ha, J. Moon, A. Faccheti, and T. J. Marks, *Adv. Mater.*, **22**, 1346 (2010).
21. J. H. Jeong, H. W. Yang, J.-S. Park, J. K. Jeong, Y.-G. Mo, H. D. Kim, J. Song, and C. S. Hwang, *Electrochem. Solid-State Lett.*, **11**, H157 (2008).
22. H. Hosono, K. Nomura, Y. Ogo, T. Uruga, and T. Kamiya, *J. Non-Cryst. Solids*, **354**, 2796 (2008).

Downloaded 13 Aug 2010 to 143.248.115.209. Redistribution subject to ECS license or copyright; see http://www.ecsdl.org/terms_use.jsp